RESEARCH ARTICLE | JANUARY 11 2024

Experimental analysis of water-droplet–fiber interaction on a mechanically excited hydrophobic fiber

A. Schwarzwaelder ; J. Meyer; A. Dittler

Physics of Fluids 36, 012010 (2024)
https://doi.org/10.1063/5.0178183

Physics of Fluids ARTICLE pubs.aip.org/aip/pof

Experimental analysis of water-droplet–fiber interaction on a mechanically excited hydrophobic fiber

Cite as: Phys. Fluids **36**, 012010 (2024); doi: 10.1063/5.0178183
Submitted: 26 September 2023 · Accepted: 18 December 2023 ·
Published Online: 11 January 2024

View Online Export Citation CrossMark

A. Schwarzwaelder,[a] J. Meyer,[b] and A. Dittler[c]

AFFILIATIONS

Institute of Mechanical Process Engineering and Mechanics, Karlsruhe Institute of Technology, 76131 Karlsruhe, Germany

[a]Author to whom correspondence should be addressed: alexander.schwarzwaelder@kit.edu
[b]Electronic mail: achim.dittler@kit.edu
[c]Electronic mail: joerg.meyer@kit.edu

ABSTRACT

In this study, the dynamics of a single water droplet on a mechanically excited single fiber are investigated fundamentally. By utilizing state-of-the-art high-speed camera technology, the droplet's motion is captured with exceptional temporal resolution, enabling a detailed analysis of its position, size, and kinetics. We can identify distinct motion patterns of a droplet adhering to the fiber, which can exhibit either a static, a tilting, or swinging motion. The swinging and tilting motion can be overlaid with a higher-frequency deformation in response to the fiber excitation. Additionally, we examine the detachment of the droplet from the fiber as well as for the first time the (periodic) reattachment resulting from the mechanical excitation. The used droplet volumes are smaller, and the excitation shown here is greater than the excitation acceleration previously investigated in single fiber studies. Insights into droplet–fiber interactions can provide a better understanding of the mechanisms occurring in coalescence filters in harsh environments, which cannot be observed *in situ* with high temporal and spacial resolution in a full-scale filter due to the lack of optical access.

NOMENCLATURE

Abbreviations

A	Amplitude (mm)
f	Frequency (Hz)
t	Time (s)
V	Volume of droplet (nl)

Greek symbols

Γ	Dimensionless acceleration
ω	Circular frequency (Hz)

I. INTRODUCTION

Droplet–fiber interactions play an important role in a variety of industrial applications. In addition to the textile industry[1,2] and fuel cell technology,[3] this includes, in particular, coalescence filtration.[4,5] In coalescence filtration, fibrous filter materials are used to filter tiny droplets, e.g., water droplets of mist, out of the gas or liquid phase.[6,7] Typically, the fibers used are glass fibers and synthetic fibers.

Reducing a coalescence separator to its core element, a single collector fiber, enables *in situ* measurements of basic droplet–fiber interactions with optical imaging methods. On a real coalescence filter, this is not possible due to the lack of optical accessibility into a fibrous material. However, with a simplified model assumption of a single fiber, it should be noted that more complex fluid structures such as liquid sails, which can be formed in coalescence filters, cannot be considered.[4]

In the literature, there are many considerations about the droplet–fiber interaction on a single static fiber. There are works on droplet deposition of individual droplets on single fibers,[8] droplet collection from mist,[9] contact angle determination of droplets on fibers,[10] droplet movement along fibers,[11] droplet detachment,[12–14] and the coalescence of multiple droplets on a fiber.[15,16]

In some of these investigations, the fiber is not at rest but set into vibration due to external forces induced by fluid flow or vibrating

devices. An improvement in separation efficiency through the mechanical excitation of a filter has already been demonstrated for dust filtration.[17]

Only a few studies are known about the fundamental mechanisms at the fiber-droplet interaction during fiber excitation. Bick *et al.*[18] examined the droplet movement on a vibrating inclined fiber. Depending on the inclination angle of a nylon fiber with a diameter of 0.35 mm and the droplet volume, they observed either a sticking behavior of the droplet, sliding along the fiber, or detachment from the fiber. Furthermore, droplet deformation on a horizontal fiber was shown using high-speed imaging. Poulain and Carlson[19] also utilized an inclined nylon fiber in their work. Their research focused on the change in contact line between the droplet and fiber during sliding along the fiber, depending on the mechanical fiber excitation. Additionally, they outline various regimes of droplet dynamics based on excitation parameters (amplitude and frequency). These regimes are categorized as harmonic pumping, sub harmonic pumping, swinging, and rocking. Harmonic pumping describes droplet deformation with the same frequency as the fiber excitation frequency. Sub harmonic pumping refers to droplet deformation at half the forcing frequency. In their work, swinging describes a movement of the droplet in the circumferential direction of the fiber, while rocking describes a droplet deformation in the axial direction of the fiber. In their case, rocking only occurs in the case of a inclined fiber and the excitation component achieved in the fiber axis direction. Even though their work could contribute significantly to the understanding of the droplet–fiber interaction, the detachment behavior under vibrating conditions and, thus, possible further mechanisms important for coalescence filtration remain unexamined. In addition to the droplet–fiber interaction of adhering droplets, this work also considers droplet detachment in more detail.

II. MATERIALS AND EXPERIMENTAL SETUP

In this study, the droplet–fiber interaction of droplets that are already deposited on a single fiber is studied. The fiber was clamped at both ends in a fiber holder (c.f. Fig. 1), which was mechanically excited with a sine wave.

A blank stainless steel fiber with a diameter of 100 μm was used. The tensile stress to clamp the fiber was 2.5 N. Demineralized water was used as the liquid medium. The static contact angle is 91° ± 3° and was determined with a droplet of 76 nl volume. The advancing and receding contact angle was determined by using the same droplet on a fiber excited by a shock. The maximum acceleration of the shock was 130 g, and the duration was 1 ms. This resulted in a displacement of the fiber of 1.6 mm. Due to the shock, the droplet begins to move along the fiber, so that advancing and receding contact angles of 139° ± 3° and 50° ± 3° were determined. All tests were carried out at room temperature (23 ± 3 °C). The droplet was applied to the fiber by discrete droplet dispensing from a piezoelectric nozzle. The piezoelectric nozzle dispensed the droplets with a volume of 0.382 nl at 200 Hz onto a spot on the fiber, so that the final droplet volume of the droplet sitting on the fiber was achieved by coalescence of a defined number of droplets. To position the nozzle relative to the fiber, it was mounted on motorized linear axes in an xyz-configuration (c.f. Fig. 2).

For the experiments with an excited fiber, four different droplet volumes were used (cf. Table I).

An electrodynamic shaker (ETS L315M) is used for the mechanical excitation of the fiber. Two amplitudes, 0.5 and 0.75 mm, were used. For each droplet volume, the fiber was excited at 40 and 100 Hz. In addition, a third frequency was investigated at which the shaker is maximally utilized. This is 172 Hz for an amplitude of 0.5 mm and 140 Hz for an amplitude of 0.75 mm. The excitation has consistently been a sine wave; however, the shaker is unable to instantaneously translate the specified sinusoidal oscillation at the required amplitude within the initial period. Instead, a startup time of 2 s was selected, during which the shaker increases the amplitude from the rest position to the desired amplitude at a constant frequency. Furthermore, the experimental setup includes a high-speed camera (*i-speed 721*) with a high magnification lens (*Navitar Zoom 6000* combined with a 3.5× extension ring). The resulting resolution from this setup is 3.1 μm px^{-1}. With this resolution, the camera can record up to 6 s in real time. A back light was chosen for the illumination so that the fiber and the droplet to be imaged can be seen as a black silhouette. Due to the short exposure time in high-speed images, a high intensity is required for the back light. The intensity was chosen in such a way that the droplet and the fiber are not overexposed and, therefore, do not appear smaller.

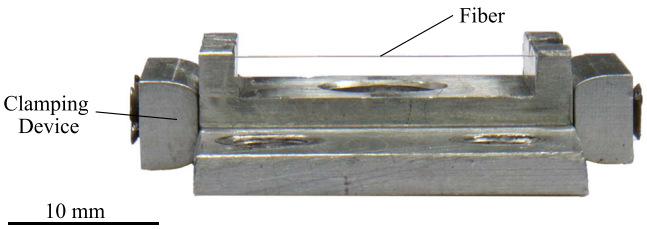

FIG. 1. Clamped fiber in the fiber holder.

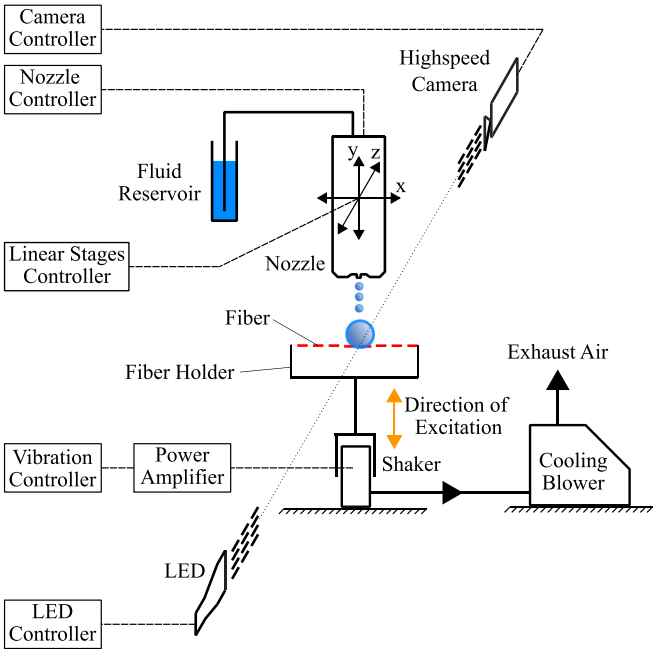

FIG. 2. Schematic diagram of the fiber vibration test system.

TABLE I. Test parameters.

Amplitude A/mm	0.5, 0.75
Frequency f/Hz	40, 100, 172 ($A = 0.5$), 140 ($A = 0.75$)
Volume of droplet V/nl	38, 76, 152, 306

III. METHOD

Each of the parameter combinations from Table I results in one experiment and was carried out 3 times. Each experiment was conducted in the same manner. First, the desired droplet volume was applied to the stationary fiber. Then, the fiber was excited with the smallest possible time delay. Since this is not an automated process, the time offset between the application of the droplet and the fiber excitation varies approximately between 3 and 5 s. The subsequent excitation time was set to 20 s. The camera trigger was activated immediately following an event, such as droplet detachment, capturing the final 6 s leading up to that event.

Due to the high frame rate of 50 000 fps, all videos were analyzed using a *MATLAB* script. The procedure was previously explained in detail in Ref. 16 and is only briefly introduced here. Figure 3 shows the main steps of the image post-processing required to track the droplets across all frames in a video.

Utilizing a threshold, the raw gray scale image of the camera is binarized. In the same step, the bright area in the droplet, which arises due to the background lighting and the refraction of light in the droplet, is removed. After that the fiber is subtracted from the image. All remaining black pixels are associated with the droplet. To the extent that there are multiple black pixel regions, segmentation is used to interpret each black area as a single droplet. Each segmented area is used as an input for the *MultiObjectTracker* in *MATLAB*. All tracked droplets are highlighted with a yellow boundary box. If a droplet is present on both the upper and lower sides of the fiber simultaneously, it is interpreted as a single connected droplet. For each detected droplet, its height, width, and area center of mass are determined. In addition, each droplet is assigned a *TrackID*, which allows a droplet to be identified as a unique object across several frames.

IV. RESULTS AND DISCUSSION

A. Static droplet and tilting motion

Depending on the excitation and the droplet volume, different states of the droplet kinetics can be identified. In the following, characteristically observed droplet dynamics are explained using selected individual experiments as examples.

For the smallest investigated droplet volume of 38 nl at a excitation frequency of 100 Hz and amplitude of 0.5 mm, the droplet adheres to the fiber. It sits almost "statically" on the fiber surface during excitation (cf. Fig. 4).

On closer inspection, a tilting motion of the droplet can be seen in the circumferential direction of the fiber. We define a tilting motion as a movement of the area center of mass $<180°$ around the fiber, while swinging represents droplet movement $>180°$ around the fiber. A deformation of the droplet is not apparent.

Figure 4 displays the temporal evolution of the spatial position of the fiber (top and bottom edges) and droplet (top and bottom edges as well as area center of mass) over time. Additionally, images of the droplet on the fiber are shown at intervals of 1 ms for one complete period. The height of the fiber (gray) plot represents the diameter of the fiber and is constant for each time step. The height of the droplet (blue) plot represents the droplet height. The start of the graph at 0 s cannot be related to the duration of the experiment, as mentioned earlier. The camera can only capture 6 s, and the trigger is activated after an event such as the droplet detachment or approximately 20 s of excitation duration if no droplet detachment is detected. It should be made clear at this point that the graph plotted in blue is not a surface but individual vertical bars for each recorded frame. This illustrates the adequate temporal resolution. It can be recognized by the plotted sinusoidal oscillation for the fiber movement (gray), and the droplet area center of mass (blue—solid line) that the slight tilting motion around the fiber is in phase with the excitation frequency.

B. Swinging motion and higher-frequency deformation

If we now look at a larger droplet with 76 nl at a higher excitation frequency of 172 Hz and the same constant amplitude of 0.5 mm, we see that the droplet swings around the fiber (cf. Fig. 5). The fact that it

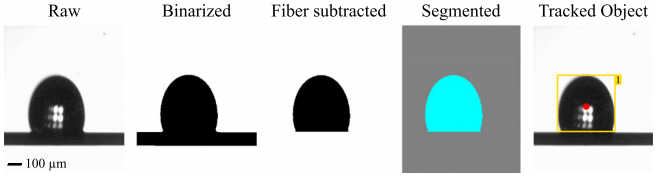

FIG. 3. Post-processing.

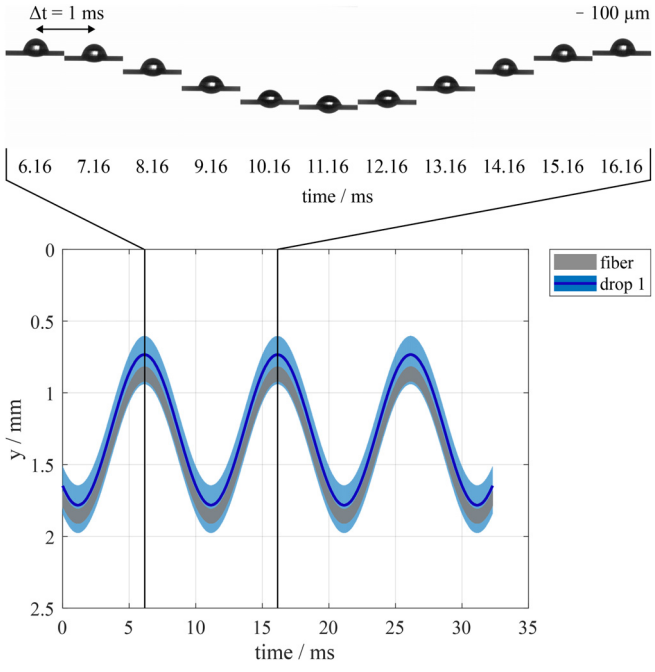

FIG. 4. Approximately static droplet with a tilting motion.

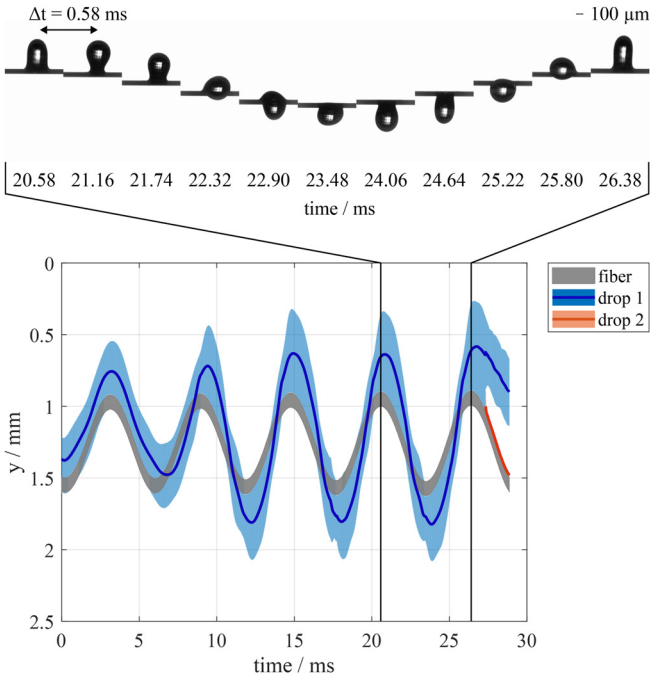

FIG. 5. Swinging and higher-frequency deformation.

is a swinging around the fiber can only be recognized from the refraction of the back light in the droplet.

In the time interval 0–6 ms, no rotation can be seen in the plot, as the blue plotted area (droplet) is above the gray plotted area (fiber). Therefore, the droplet sits on the fiber. Only when the fiber is at its lowest position at approximately 6 ms does the droplet start to roll around the fiber. In the time interval 6–26 ms, the droplet continues to swing around the fiber. The swinging is almost in phase with the excitation. This means, at the upper inversion point of the fiber, the droplet is above the fiber, and at the lower inversion point of the fiber, the droplet is below the fiber.

The area center of mass for the droplet also shows that it moves further and further away from the fiber as the test time progresses. A constant orbital frequency, leading to a consistent angular velocity, coupled with the increasing displacement of the droplet's center of mass from the fiber axis, results in a rising centrifugal acceleration.

It can also be seen from the droplet height in the graph that there is a droplet deformation. With a pure swinging around the fiber, there would be no change in the droplet height at the lower reversal point of the fiber, for example, at 23.5 ms. Thus, there must be two different droplet dynamics, swinging around the fiber and a higher-frequency deformation.

Ultimately, the droplet detaches from the fiber after several periods and three droplet revolutions at 27.28 ms. After the droplet has detached, a liquid residue remains on the fiber, which is recognized as a new second droplet (orange).

C. Detachment

Figure 6 shows the end of the detachment process of the previously described experiment in detail. The droplet initially oscillates around the fiber.

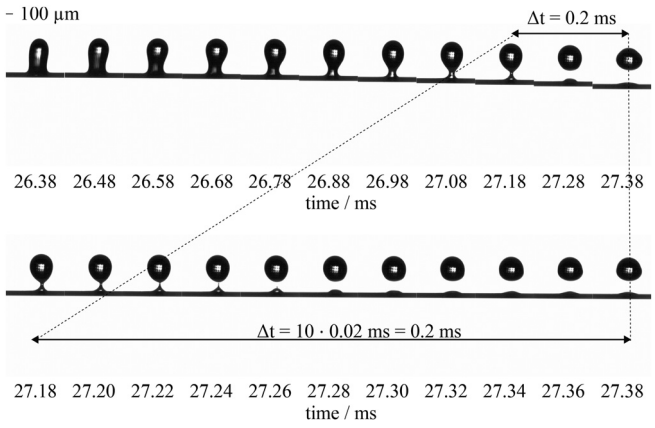

FIG. 6. Droplet detachment after higher-frequency deformation and swinging around the fiber.

At the upper reversal point of the fiber, the center of mass of the droplet continues to move upward due to the small phase shift between the swinging motion of the droplet and the vibration of the fiber. At the same time, the fiber starts to move downward. This contrary motion causes an elongated droplet shape, which starts to constrict. The necking progresses fastest near the fiber. At the time right before the droplet break-off, the primary droplet has an almost spherical shape. At the point of contact with the fiber, a formation of a liquid accumulation with a respective contact angle occurs as a result of the wetting properties. The primary droplet and this liquid collection are connected by a liquid bridge. At the time of the droplet break-off, the liquid bridge finally constricts at the contour of the primary droplet, and the liquid components of the liquid bridge are drawn toward the fiber so that a liquid residue remains on the fiber.

For a larger droplet with 152 nl at the same excitation of $A = 0.5$ mm and frequency of $f = 172$ Hz, it can be seen that the constriction of the droplet creates a satellite droplet (c.f. Fig. 7).

This satellite droplet is caused by the fact that the liquid bridge is now longer than in the previously shown example from Fig. 6, and the liquid bridge now collapses at two locations. On the one hand, the liquid bridge collapses as described earlier at the transition point between

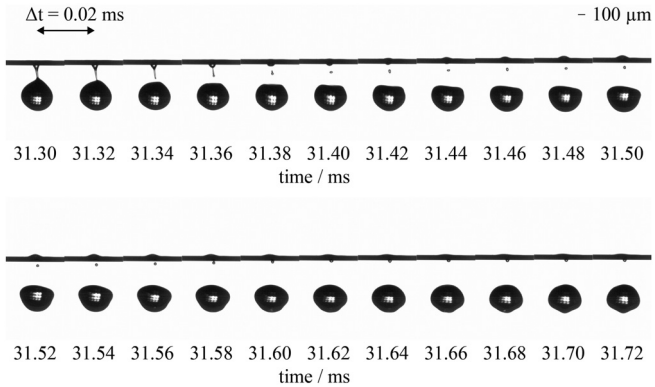

FIG. 7. Detachment with the generation of satellite droplet.

the liquid bridge and the primary droplet, which has an almost spherical shape, and on the other hand, it collapses near the transition point between the liquid bridge and the liquid accumulation on the fiber, which arises due to the fiber wettability. The diameter of the satellite droplet, averaged over all frames in which it can be seen, is 25 μm, 8.2 pl. Again, a liquid residue remains on the fiber. Following the detachment of the droplet, the residual liquid is transported around the fiber and, based on the 2D view, appears to be located on the opposite side of the fiber at the end of the observed process. The satellite droplet moves toward the fiber due to the resulting impulse. At the end of the detachment process, the satellite droplet has been deposited on the fiber and is located opposite to the liquid residue.

In the context of the filtration application, the generation of satellite droplets is problematic. In most cases, the satellite droplet falls back onto the fiber, but it has also been observed in experiments that the droplet can be emitted into the atmosphere. It is assumed that the satellite droplet does not fall back onto the fiber if the surrounding gas phase is not at rest, but there is an incident flow. In addition, there is also the possibility that the resulting momentum of the satellite droplet after the liquid bridge collapses is so small that it moves very slowly (if at all) toward the fiber. If the fiber exhibits a comparatively fast oscillating motion, the droplet will fail to hit the fiber and will not be deposited on it again, except for the fact that the gravitational force is directing the droplet toward the fiber. However, to confirm this, the process must be observed from the axial fiber direction with and without an incident flow.

D. Reattachment

For even larger droplets of 306 nl and again the same constant amplitude of 0.5 mm and the same frequency of 172 Hz, a periodic detachment and reattachment of the droplet can be seen. According to Fig. 8, the droplet detaches in this experiment without depending on an underlying swinging motion of the droplet around the fiber. Instead, in this case, the droplet is pushed away from the vibrating fiber. As a result, the droplet deforms and detaches from the fiber. However, the droplet is not repelled far enough within a period of a fiber oscillation and is deposited on the fiber again.

In order to better illustrate the process of periodic reattachment, only a section of the entire recorded video is shown here in Fig. 8.

After further cycles, not shown here, in which the drop adheres to the fiber over several periods of fiber oscillation, the drop finally detaches and is emitted into the environment. In conclusion, at the end of an experiment monitoring droplet reattachment, the primary droplet eventually always detached from the fiber. No satellite droplets could be observed during this experiment. However, in principle, there is a risk of satellite droplet generation at every single detachment event.

V. CONCLUSIONS

In conclusion, there are clearly distinguishable dynamics that the droplet can perform. The droplet dynamics include an "approximately static droplet dynamics" for the smallest droplets or low values of Γ and with increasing excitation a tilting movement. In addition, the droplet can exhibit a swinging motion around the fiber. Higher-frequency deformation can occur simultaneously, when the droplet exhibits a swinging or tilting motion. These droplet dynamics were

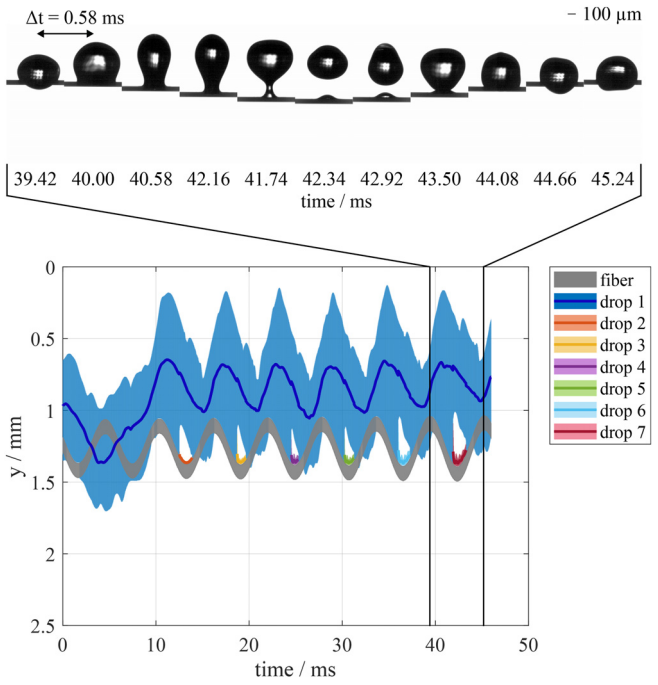

FIG. 8. Droplet reattachment.

exemplified with selected experiments. Furthermore, reattachment was demonstrated for the first time. This should be avoided in a coalescence filter, as, in principle, every detachment process can be accompanied by the emission of a satellite droplet into the atmosphere. After exemplifying the possible droplet dynamics, the respective droplet behaviors for the entire examined parameter space are now determined and classified.

Figure 9 shows, for all the tests carried out, whether the droplet detaches and, if so, with or without a satellite droplet, whether the detached main droplet reattaches. After sufficient excitation time, a reattached droplet is always finally detached and has been emitted into the environment. Here, the dimensionless acceleration $\Gamma = A \cdot \omega^2/g$ is plotted against the droplet volume, where $\omega = 2\pi f$. The dimensionless

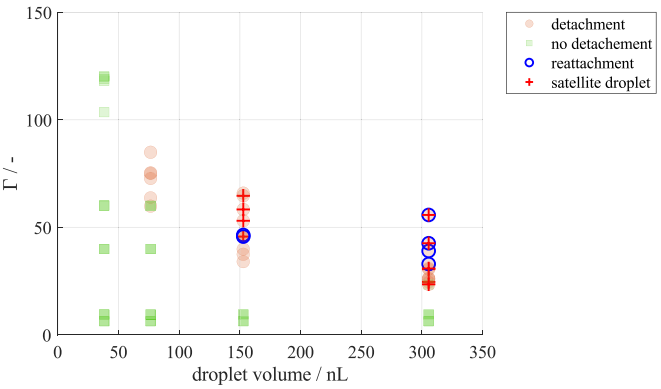

FIG. 9. Overview of the outcome of the droplet–fiber interaction after excitation.

acceleration Γ describes the excitation by including the amplitude and frequency.

For droplet volumes of 38 nl, no detachment was observed. For droplet volumes of 76 nl, detachment was observed at $\Gamma > 60$, and no satellite droplets were observed. As the droplet volume increases, detachment occurs at smaller Γ values. Additionally, for droplet volumes of 152 and 306 nl, satellite droplets were also observed during detachment. Reattachment was observed preferentially for very large droplet volumes, since these heavier droplets accelerate slower and are therefore "recaptured" by the fiber.

Limitations of this work relate, in particular, to the uncontrolled influencing parameters that affect the evaporation of the water droplet. These include the ambient conditions (temperature and air pressure) and the temperature of the fiber holder. In addition, the accuracy of the evaluation is limited by the resolution of 3.1 μm px^{-1} and the setting of the threshold for binarisation. Objects (satellite drops) smaller than this size cannot be detected. In addition, due to the radial approach, no clear information can be provided about the rotational movement of the droplet (e.g., relative speed of the area center of mass of the fiber to the droplet in the circumferential direction).

VI. OUTLOOK

Further studies will be carried out for a wettable system. Oil should be used as a medium to reduce evaporation effects. In addition, due to the radial viewing direction, it is not possible to clearly distinguish the rotational motion of the droplet from the deformation. Further experiments will be conducted from an axial viewpoint. In addition, the tests must be extended to a multifiber arrangement and, finally, to a full filter media section, in order to be able to trace the effect of the mechanisms observed here on the filter efficiency.

ACKNOWLEDGMENTS

We wish to confirm that there are no known conflicts of interest associated with this publication. We confirm that the manuscript has been read and approved by all named authors, and that there are no other persons who satisfied the criteria for authorship but are not listed. We further confirm that the order of authors listed in the manuscript has been approved by all of us. The authors have no relevant financial or non-financial interest to disclose. We gratefully acknowledge that this project was funded by the Deutsche Forschungsgemeinschaft (DFG, German Research Foundation)–DFG/499469405. In closing, we would like to express our sincere appreciation and recognition for the extensive work of Edhem Acunman. This research has been greatly enriched by his dedicated and skilled contributions in the laboratory.

AUTHOR DECLARATIONS

Conflict of Interest

The authors have no conflicts to disclose.

Author Contributions

Alexander Wilhelm Schwarzwaelder: Writing – original draft (equal). **Jörg Meyer:** Writing – review & editing (supporting). **Achim Dittler:** Writing – review & editing (supporting).

DATA AVAILABILITY

The data that support the findings of this study are available from the corresponding author upon reasonable request.

REFERENCES

[1]S. Michielsen and H. J. Lee, "Design of a superhydrophobic surface using woven structures," Langmuir **23**, 6004–6010 (2007).
[2]D. Chen, L. Tan, H. Liu, J. Hu, Y. Li, and F. Tang, "Fabricating superhydrophilic wool fabrics," Langmuir **26**, 4675–4679 (2010).
[3]E. Gauthier, T. Hellstern, I. G. Kevrekidis, and J. Benziger, "Drop detachment and motion on fuel cell electrode materials," ACS Appl. Mater. Interfaces **4**, 761–771 (2012).
[4]C. Straube, J. Meyer, and A. Dittler, "Identification of deposited oil structures on thin porous oil mist filter media applying μ-CT imaging technique," Separations **8**, 193 (2021).
[5]S. Wurster, J. Meyer, H. E. Kolb, and G. Kasper, "Bubbling vs. blow-off - On the relevant mechanism(s) of drop entrainment from oil mist filter media," Sep. Purif. Technol. **152**, 70–79 (2015).
[6]X. Yang, X. Zhang, H. Wang, and G. G. Chase, "Vibration assisted water-diesel separation by electrospun PVDF-HFP fiber mats," Sep. Purif. Technol. **171**, 280–288 (2016).
[7]X. Yang, H. Wang, and G. G. Chase, "Performance of hydrophilic glass fiber media to separate dispersed water drops from ultra low sulfur diesel supplemented by vibrations," Sep. Purif. Technol. **156**, 665–672 (2015).
[8]S. Abishek, R. Mead-Hunter, A. J. King, and B. J. Mullins, "Capture and re-entrainment of microdroplets on fibers," Phys. Rev. E **100**, 042803 (2019).
[9]R. Labbé and C. Duprat, "Capturing aerosol droplets with fibers," Soft Matter **15**, 6946–6951 (2019).
[10]N. M. Farhan, H. Aziz, and H. V. Tafreshi, "Simple method for measuring intrinsic contact angle of a fiber with liquids," Exp. Fluids **60**, 87 (2019).
[11]T. Gilet, D. Terwagne, and N. Vandewalle, "Droplets sliding on fibres," Eur. Phys. J. E **31**, 253–262 (2010).
[12]N. M. Farhan and H. V. Tafreshi, "Using magnetic field to measure detachment force between a nonmagnetic droplet and fibers," Langmuir **35**(25), 8490–8499 (2019).
[13]N. M. Farhan and H. Vahedi Tafreshi, "Universal expression for droplet-fiber detachment force," J. Appl. Phys. **124**, 075301 (2018).
[14]N. Ojaghlou, H. V. Tafreshi, D. Bratko, and A. Luzar, "Dynamical insights into the mechanism of a droplet detachment from a fiber," Soft Matter **14**, 8924–8934 (2018).
[15]Y. Jiang, L. Feng, A. O'Donnell, C. MacHado, W. Choi, N. A. Patankar, and K. C. Park, "Coalescence-induced propulsion of droplets on a superhydrophilic wire," Appl. Phys. Lett. **121**, 231602 (2022).
[16]A. Schwarzwälder, J. Meyer, and A. Dittler, "Experimental analysis of droplet coalescence and transport mechanisms on a single vertical fiber," Exp. Fluids **64**, 103 (2023).
[17]S. C. Kim, H. Wang, M. Imagawa, D.-R. Chen, and D. Y. H. Pui, "Experimental and modeling studies of the stream-wise filter vibration effect on the filtration efficiency," Aerosol Sci. Technol. **40**, 389–395 (2006).
[18]A. Bick, F. Boulogne, A. Sauret, and H. A. Stone, "Tunable transport of drops on a vibrating inclined fiber," Appl. Phys. Lett. **107**, 181604 (2015).
[19]S. Poulain and A. Carlson, "Sliding, vibrating and swinging droplets on an oscillating fibre," arXiv:2210.06314.